Journal of Alloys and Compounds 526 (2012) 110–115

Contents lists available at SciVerse ScienceDirect

Journal of Alloys and Compounds

journal homepage: www.elsevier.com/locate/jallcom

# Development of wide band gap sensor based on $AlNbO_4$ nanopowder for ethanol

C. Balamurugan [a], A. Subashini [a], G.N. Chaudhari [b], A. Subramania [c,*]

[a] Department of Industrial Chemistry, Alagappa University, Karaikudi – 630 003, India
[b] Department of Chemistry, Shri Shivaji Science College, Amravati – 444 603, India
[c] Centre for Nanoscience and Technology, Pondicherry University, Puducherry – 605 014, India

ARTICLE INFO

*Article history:*
Received 22 August 2011
Received in revised form 13 January 2012
Accepted 16 January 2012
Available online xxx

*Keywords:*
$AlNbO_4$
Niobium–citrate process
Nanopowder
Ethanol sensor
Gas sensor
Diffuse reflectance spectra

ABSTRACT

Aluminium niobate ($AlNbO_4$) nanopowder was synthesized by niobium–citrate complex process and characterized by thermal analysis (TG/DTA), X-ray powder diffraction (XRD), scanning electron microscopy (SEM), transmission electron microscope (TEM) and energy dispersive X-ray spectroscopy (EDX), diffuse reflectance spectra (DRS), impedance analysis and Brunauer–Emmett–Teller (BET). The well crystalline orthorhombic $AlNbO_4$ was obtained by heat treatment at 900 °C. TEM results indicated that the average size of the rectangle shaped $AlNbO_4$ particles was 30 nm width and 60 nm length. The optical band gap of the nanopowder was estimated to be 3.63 eV. The temperature dependent conductivity of $AlNbO_4$ was found to obey an Arrhenius relation with an activation energy value of 0.26 eV. The gas sensing behaviour of $AlNbO_4$ nanopowder was analysed by measuring the changes in resistance of the sensor material in presence of each reducing gas such as ethanol, liquid petroleum gas and ammonia as a function of the operating temperatures, gas concentrations and the response time. The $AlNbO_4$ nanopowder showed good sensitivity for ethanol (99%) rather than LPG (43%) and $NH_3$ (19%) at an operating temperature of 250 °C.



## 1. Introduction

Due to its enhanced sensitivity, the development of semiconductor metal oxide sensors is of continued interest. Mesoporous $Nb_2O_5$ has attracted much attention because of its special properties and applications in electrochromic, photocatalytic hydrogen production, gas sensors, electrocatalysis, and porous coating in electrochemical solar cells [1–5] etc. One of the important approaches to enhancing sensitivity is surface modification by proper choice of additives or dopants to the base oxide materials. Transition metals have been used as successful doping materials for $Nb_2O_5$, which increased the resistivity of $Nb_2O_5$ due to the depressed carrier concentrations. The resistivity enhanced the sensitivity of metal oxide based gas sensor. Niobium based binary metal oxides such as $FeNbO_4$, $InNbO_4$, $CrNbO_4$, $CeNbO_4$ and $LaNbO_4$ are being studied extensively, exhibit interesting structural, chemical, electrical and optical properties [6–10]. They were mostly prepared by solid state reaction method. The preparation method and choice of metal precursor has important effects on the dispersion, specific surface area, morphology, and other structural properties of metal oxides, which influence the sensor performance. The sensing mechanism is based on the surface reaction of the particles with the exposed gas by adsorption and desorption mechanism. The adsorption being a surface effect, surface area plays an important role in the sensing mechanism. In the nanosized materials, a large fraction of the atoms are present at the surface, and are widely used to enhance the gas-sensing properties of semiconducting oxides. In the present investigation, we report the synthesis of $AlNbO_4$ nanopowder by niobium–citrate complex process. The prepared $AlNbO_4$ nanopowder was subjected to TG/DTA, XRD, SEM, TEM, DRS and BET characterization. The sensitivity of $AlNbO_4$ based sensor was studied by measuring the resistance of the sensor in air and in the reducing gas environments such as ethanol ($C_2H_5OH$), liquid petroleum gas (LPG) and ammonia ($NH_3$).

## 2. Experimental

### 2.1. Preparation of $AlNbO_4$ nanopowder

$AlNbO_4$ nanopowder was obtained by low temperature niobium–citrate complex process using the following two steps: the first step was the preparation of hydrated $Nb_2O_5$ from $Nb_2O_5$. $Nb_2O_5$ was dissolved in HF to form $[NbOF_5]^{2-}$ or $[NbF_7]^{2-}$ complex [11]. A freshly prepared aqueous solution of ammonium oxalate was added in excess and then aqueous $NH_3$ was added drop by drop to get hydrous niobium oxide ($Nb_2O_5 \cdot nH_2O$) as precipitate. The hydrous oxide precipitate was then filtered and washed with 10% aqueous $NH_3$ solution by centrifugation to make the solution, fluoride free hydrated $Nb_2O_5$. In the second step, the stoichiometric amount of hydrated $Nb_2O_5$ was dissolved in the aqueous solution of citric acid (2 mol/mol of niobium ion) with the addition of catalytic amount of hydrogen

* Corresponding author. Tel.: +91 0413 2654980; fax: +91 0413 2654612.
*E-mail addresses:* a_subramania@yahoo.co.in, a.subramania@gmail.com (A. Subramania).

0925-8388/$ – see front matter © 2012 Elsevier B.V. All rights reserved.
doi:10.1016/j.jallcom.2012.01.085

peroxide, to get clear yellow coloured peroxo-citro-niobate. The addition of $H_2O_2$ promoted the solubility of the hydrated niobate in citric acid and also shortened the required dissolution time. The clear solution of peroxo-citro-niobiate was mixed with stoichiometric amount of aluminium nitrate (mole ratio of Al/Nb = 1:1) with constant stirring. The pH of the final solution mixture was adjusted to 7 by addition of aqueous $NH_3$. This mixture was heated at about 200 °C to get a dried black fluffy mass. This dried mass was calcined at 900 °C for 2 h to get $AlNbO_4$ nanopowder. The resultant product was collected and subjected into both physical characterization and gas sensor studies.

### 2.2. Physical characterization studies

The thermal decomposition behaviour of the as-prepared powder was characterized by thermogravimeteric and differential thermal analysis (TG/DTA) under air atmosphere to find out the phase formation temperature of the precursor sample. The analysis was carried out in the instrument using thermal analyzer (Model: Pyris Diamond) at the heating rate of 10 °C/min from 30 to 900 °C. Another part of the as-prepared black carbonaceous $AlNbO_4$ powder was calcined at 600 °C, 700 °C, 800 °C and 900 °C for 2 h. The phase identification of the calcinated powder was performed using X-ray diffractometer (Model: X' pert-pro diffractometer) using nickel filtered (Cu-$K_\alpha$) radiation as the source and operated at 40 kV. The sample was scanned in the $2\theta$ range from 10° to 70° with 0.02° step. The morphology of the powder was observed using scanning electron microscope (Model: Hitachi, SN-3400N). The particle size and compositional analyses were carried out using transmission electron microscopy (Model: Philips CM-20) and energy dispersive spectroscopy attached with TEM. For TEM investigation, an ultrasound bath was used to disperse the $AlNbO_4$ powder in ethanol. A drop of this suspension was placed in a carbon coated copper grid. After evaporation of the ethanol, the particles were viewed in the TEM. The optical characterization was carried out using UV–vis absorption spectra (Model: Varian, Cary-5000) equipped with a diffuse reflectance accessory. The surface area of $AlNbO_4$ powder was measured by BET (Micrometrisics, ASAP 2020) nitrogen adsorption and desorption method at −196 °C. For conductivity studies, the synthesized $AlNbO_4$ nanopowder was mixed with a few drops of polyvinyl alcohol solution, and the mixture was pressed into a pellet of 10 mm diameter with 1.5–2 mm thickness using a die at 150 MPa. The pellet was then heat-treated at 400 °C to remove the residual polymer which was added to produce a porous solid. Conductivity of pellet was measured with the help of stainless steel blocking electrodes using a computer-controlled Potentiostat/Galvanostat (Model: micro auto lab type III) in the frequency range of 1 Hz–500 KHz at 30–175 °C.

### 2.3. Gas sensor studies

For gas sensing properties, the calcined $AlNbO_4$ nanopowder was mixed with 2% polyvinyl alcohol to make a paste. The paste was coated on a ceramic tube substrate and the thickness of the coating was 30 μm this was annealed at 500 °C for 2 h to make it rigid and to impart porous properties. The tube was about 8 mm in length, 2 mm in external diameter and 1.6 mm in internal diameter, equipped with two platinum wire electrodes (8 mm) for electrical contacts. For gas sensing measurements, the sensor element was provided with a heater fixed inside the ceramic tube coated with the sensor material. A Cr–Al thermocouple was used to sense the operating temperature of the test chamber. The test gas was injected into the test chamber through an injection part and the electrical resistance of the sensor was measured as a function of time till a constant value was attained. The chamber was then purged with fresh air for about 10 min and the experiment was repeated. The electrical resistance of the sensor in the absence of gas was also measured by means of conventional circuit in which the load resistor was connected in series at a circuit voltage of 10 V. The value of the sensor resistance was measured by monitoring the output voltage across the load resistor changed with the concentrations of the test gases. The electrical resistance was measured both in the presence and absence of the test gas. The sensor response ($S$) was calculated using the following equation [12];

$$S(\%) = \frac{R_a - R_g}{R_a} \times 100$$

where, $R_a$ is the resistance of the sensor in air and $R_g$ is the resistance of sensor in the presence of the test gas. The gas sensing properties of reducing gases such as LPG, $NH_3$ and $C_2H_5OH$ were measured in different temperatures ranging from 50 to 350 °C at gas concentrations of 100–700 ppm.

## 3. Results and discussions

### 3.1. Thermal studies

Fig. 1 shows simultaneous TG/DTA plots obtained for the $AlNbO_4$ precursor sample. The DTA plot show two endothermic peaks at 147 °C and 250 °C due to the removal of the water molecules in the sample and thermal decomposition of free citric acid and respectively, their corresponding weight loss was observed in the TG plot.

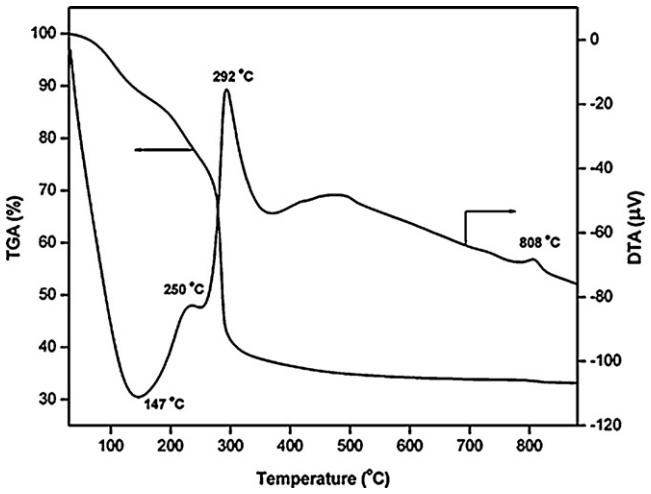


**Fig. 1.** TG/DTA curves of $AlNbO_4$ precursor.

The first sharp exothermic peak at 292 °C could be due to the reaction of nitrates with citric acid. This reaction, generate an enormous amounts of heat energy and liberate large amount of gases such as $CO_2$, $N_2$, and water vapour. This resulted, a considerable weight loss in the TG plot. The second broad exothermic peak appears at around 388 °C and terminates at around 500 °C with weight loss in TG plot. This is due to the burning of the remaining organic constituents in the precursor. Above 500 °C, there is no significant thermal effect observed in the TG/DTA curve, which indicates that the decomposition of the precursor is completed by 500 °C. As the process of heating was continued, the DTA showed one weak exothermic peak at 808 °C with a small weight loss in TG is due to the structural changes of $AlNbO_4$ from the monoclinic to the orthorhombic. This structural changes is further confirmed by the XRD data. TG/DTA measurements are used to find out the optimum calcination temperature to get phase pure product. For $AlNbO_4$, the calcination temperature was normally between 600 °C and 900 °C.

### 3.2. X-ray diffraction studies

Fig. 2 depicts the X-ray diffraction patterns of $AlNbO_4$ powder calcined at various temperatures (600–900 °C for 2 h). Fig. 2(a) shows the amorphous structure when it was calcined at 600 °C. Crystallization occurs at 700 °C. The sample calcined at temperature 800 °C exhibited $AlNb_{49}O_{129}$ monoclinic phase [13]. This observation indicates that the reaction was incomplete. When the calcination temperature reached 900 °C, single phased $AlNbO_4$ was obtained and all of the reflection peaks were indexed as a pure orthorhombic phase of $AlNbO_4$ (JCPDS Card No. 26-0030) and no characteristic peaks for impurities were observed. The calculated lattice parameters, $a = 6.15 \pm 0.02$ Å, $b = 7.40 \pm 0.02$ Å and $c = 8.60 \pm 0.01$ Å of the sample were closely matched with the standard lattice parameters. The observed peaks became sharper, when the calcination temperature was raised to 900 °C, suggesting a gradual growth in the average particle size and also an increase in the crystallinity of $AlNbO_4$ powder. The average crystallite size of $AlNbO_4$ calcined at 900 °C for 2 h was calculated using Scherrer equation and it was found to be 70 nm. $AlNbO_4$ had two polymorph phases. The XRD pattern showed the monoclinic phase at the calcination temperature of 800 °C and it changed into the orthorhombic phase at the calcination temperature of 900 °C.

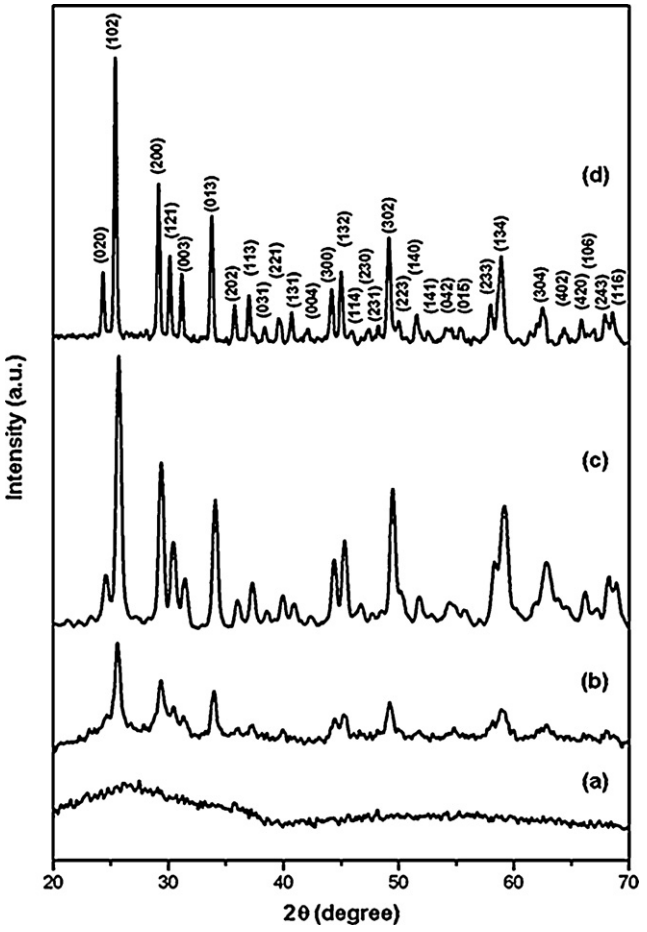


**Fig. 2.** X-ray diffraction patterns of $AlNbO_4$ precursor powder calcined at (a) 600, (b) 700, (c) 800, and (d) 900 °C for 2 h.

### 3.3. SEM studies

Fig. 3 shows the SEM morphology of the $AlNbO_4$ calcined at 900 °C for 2 h. It shows that some of the particles combined with each other and leaving some spaces as pores. These pores can act as a channel for the diffusion of gas and provide more active sites. This may improves the reaction of gas with surface adsorbed oxygen. These features make the $AlNbO_4$ better for gas sensing applications.

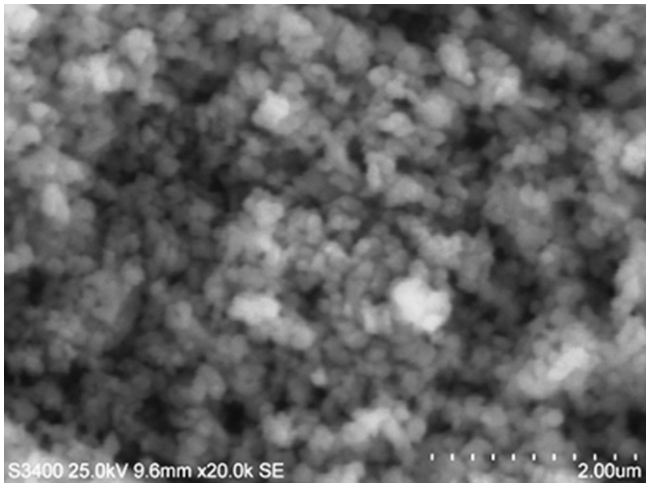


**Fig. 3.** Scanning electron micrograph of $AlNbO_4$ nanopowder obtained at 900 °C.

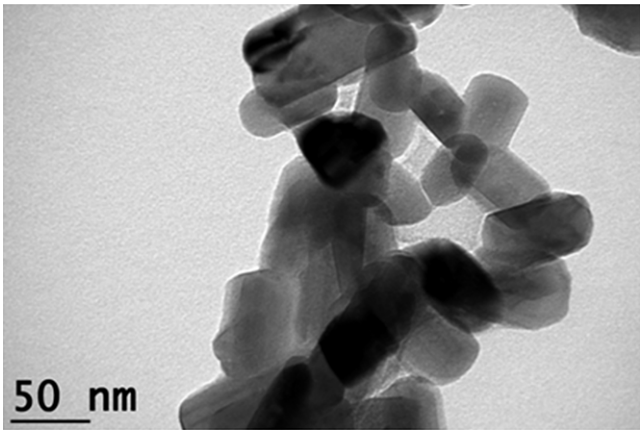


**Fig. 4.** Transmission electron micrograph of $AlNbO_4$ nanopowder obtained at 900 °C.

### 3.4. TEM studies

The TEM image of $AlNbO_4$ powder is shown in Fig. 4. The rectangular shape with round corners of the particles was seen with negligible amount of agglomeration. The size of the particles were mostly uniform they were homogeneously distributed with distinguishable grain boundaries. The average size of the rectangle shape $AlNbO_4$ was 30 nm in width and 60 nm in length. The selected area electron diffraction (SAED) pattern was obtained for the prepared $AlNbO_4$ as shown in Fig. 5. This showed that the powder is well crystalline, and the observed rings confirmed the presence of crystal lattice of (2 0 0), (2 1 2) and (4 0 0) orientation. It revealed the orthorhombic phase of the sample.

### 3.5. EDX studies

The EDX result showed the elemental composition of $AlNbO_4$ nanopowder (Fig. 6). The atomic % for Al, Nb and O were found out from the EDX and was 17.30, 17.70 and 65.00, respectively which was very close to the stoichiometric ratio of pure $AlNbO_4$. This result was consistent with X-ray diffraction analysis of the sample with phase corresponding to $AlNbO_4$. The oxygen content of the sample was found to be less than stoichiometric content. This deficiency made the material useful in sensor applications.

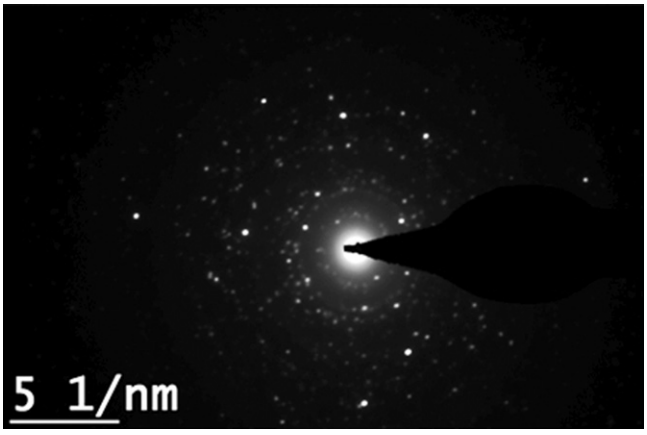


**Fig. 5.** SAED pattern of $AlNbO_4$ nanopowder.

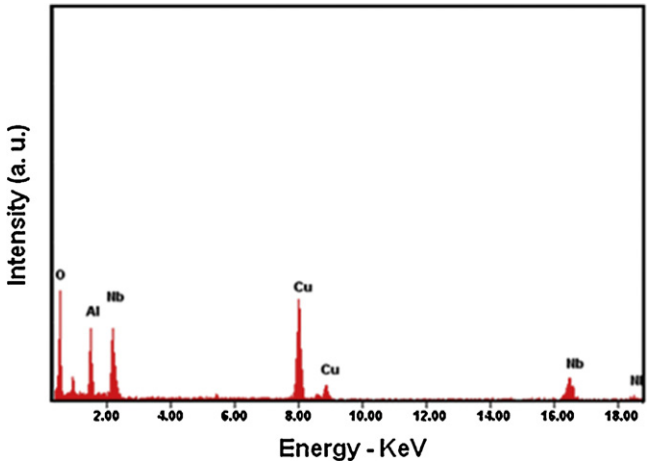


**Fig. 6.** EDX analysis of $AlNbO_4$ nanopowder calcined at 900 °C.

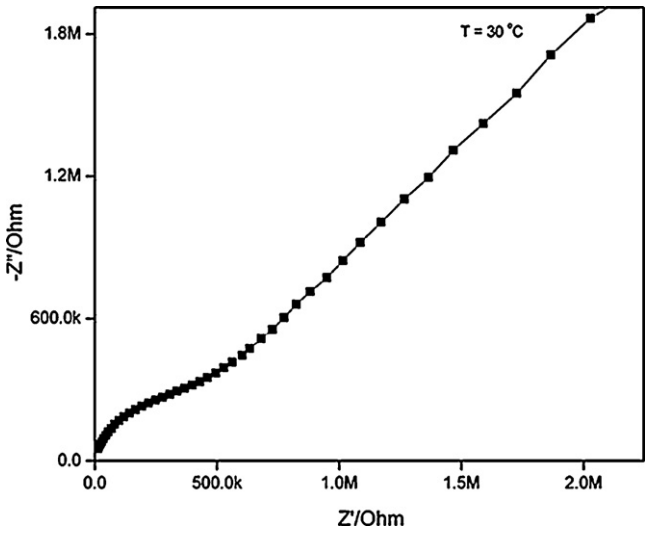


**Fig. 8.** Impedance spectrum of $AlNbO_4$ nanopowder calcined at 900 °C.

### 3.6. Diffuse reflectance spectra studies

Fig. 7 shows the diffuse reflectance spectrum of $AlNbO_4$ nanopowder. The intercept of the tangent to the plot, absorption versus wavelength gives the absorption edge ($\lambda$) of the sample and it was 341 nm. From this, optical band gap, $E_g$ value was calculated using the following relation [14];

$$E_g = \frac{hc}{\lambda}$$

where $h$ is the Plank's constant ($6.602 \times 10^{-34}$), $C$ is the velocity of light ($3 \times 10^8$). The band gap was found to be 3.63 eV.

### 3.7. Impedance studies

The complex impedance plot of the $AlNbO_4$ nanopowder at 30 °C is shown in Fig. 8. The semicircular portion at the higher frequency region disappears indicating that the conductivity depends mainly on the grain boundary response. The electrical conductivity, $\sigma$ can be estimated from the following relation;

$$\sigma = \frac{L}{RA}$$

where $\sigma$ is the electrical conductivity, $L$ is the thickness and $A$ is the surface area of the sample, $R$ is the resistance of the sample obtained from complex impedance plot. It is widely accepted that $R$ could be obtained from the intercept on the $x$-axis at the high frequency end of the complex impedance [15,16]. The variation in log $\sigma$ with inverse of temperature was plotted in Fig. 9. Conductivity increased with temperature. The temperature dependent conductivity values obey the Arrhenius relation. This was mainly due to the deficiency of the oxide ion which suggests that the loss of one oxide ion from the lattice created one oxide ion vacancy, leaving two electrons. This may be represented by the reaction;

$$O_o \rightarrow \tfrac{1}{2}O_2 + V_o^{\bullet\bullet} + 2e^-$$

The number of vacancies created (0.08 per formula unit) could be related with 0.16 Nb(V) ions reduced to Nb(IV) per formula unit. The oxygen deficiency was confirmed by the EDX spectrum. This result is well correlated with the EDX results. Therefore, individual oxygen vacancies, $V_o^{\bullet\bullet}$ and the vacancies stabilized with the reduction of Nb(IV) ions seem to respond in the conductivity process [7,17]. The activation energy was calculated from the slope of log $\sigma$ versus $1/T$ plot. In the temperature studied range, the activation energy of $AlNbO_4$ was found to be 0.26 eV.

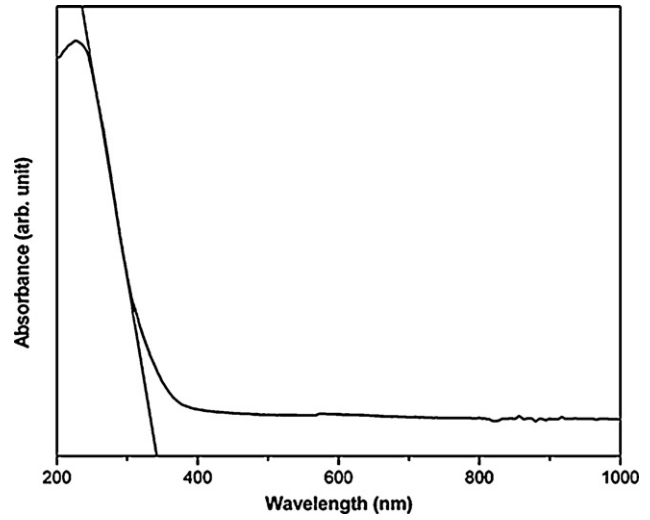


**Fig. 7.** Diffuse reflectance spectrum of $AlNbO_4$ nanopowder.

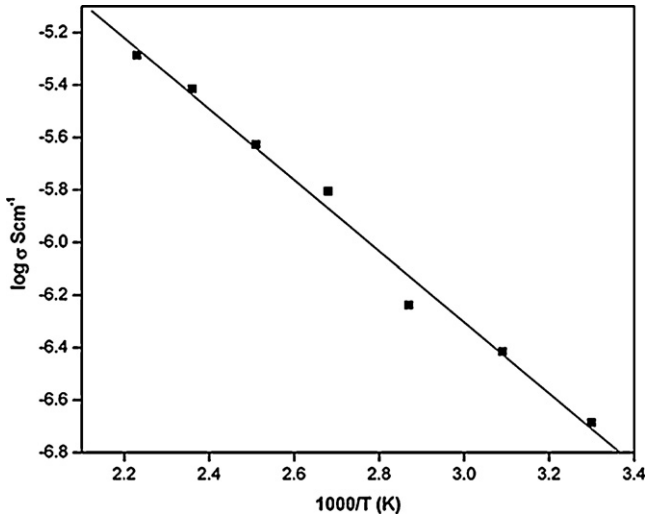


**Fig. 9.** Arrhenius plot of log conductivity versus reciprocal temperature for $AlNbO_4$.

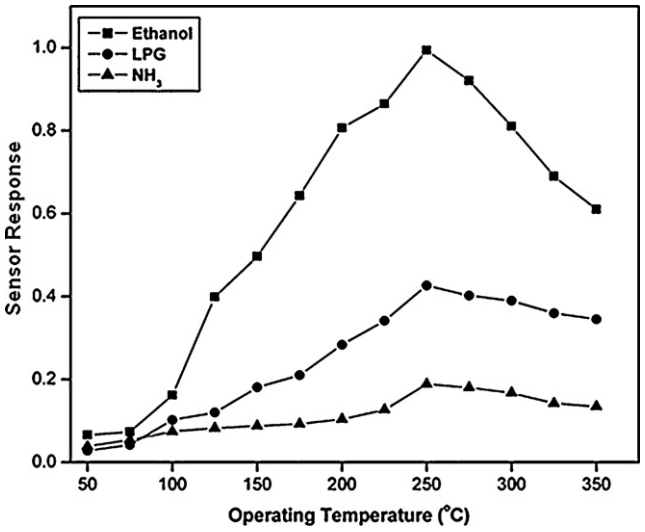


**Fig. 10.** Response of $AlNbO_4$ sensor as a function of various operating temperatures for $C_2H_5OH$, LPG and $NH_3$ gases.

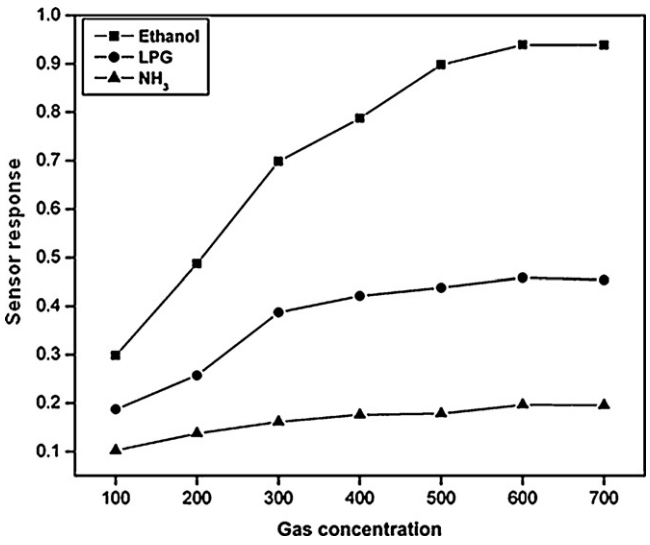


**Fig. 11.** Response of $AlNbO_4$ sensor with the different concentrations of $C_2H_5OH$, LPG and $NH_3$ at their optimum operating temperatures.

### 3.8. BET specific surface area studies

The specific surface area of $AlNbO_4$ nanopowder calcined at 900 °C was measured by using nitrogen adsorption BET method, and it was 28.36 $m^2/g$.

## 4. Gas sensing studies

### 4.1. Sensor response with operating temperatures

$AlNbO_4$ based sensor was subjected to gas sensor studies with the test gases such as $C_2H_5OH$, $NH_3$ and LPG by measuring sensor response as a function of various operating temperatures are presented in Fig. 10. The optimum sensing temperature was obtained from the plot of sensor response as a function of operating temperature. From the Fig. 10, it may be clear the sensitivity of this sensor was remarkably higher for $C_2H_5OH$ (99%) than LPG (43%) and $NH_3$ (19%) at 250 °C. For these experiments, the resistance was measured by cooling the sample after being heated to sufficiently high temperatures, thereby securing a good reproducibility of the sensitivity temperature characteristics. When the operating temperature was raised, the sensitivity for ethanol gas slowly increased, to reach a maximum at 250 °C. Then the sensitivity decreased with further rises in temperature. This might be due to the increase of desorption kinetics on the surface of the sensor material at above 250 °C. Besides this, the physical properties of the semiconducting sensor material such as charge carriers and Debye length were also influenced by temperature [18]. Hence, the optimum working temperature was fixed as 250 °C to proceed the subsequent detections.

### 4.2. Sensing mechanism

$AlNbO_4$ based sensor response was due to surface interaction between the metal oxide and the surrounding gases, such as oxygen from the air adsorbed on to the surface of the $AlNbO_4$. The form of the adsorbed oxygen depends on temperature of the sensor, at high temperatures $O^-$ and $O^{2-}$ are commonly chemisorbed [19]. When reducing gases are introduced, it reacts with the oxygen absorbed on the surface of $AlNbO_4$ and the electrons captured by the oxygen return to the $AlNbO_4$ material, resulting in the change in resistance of $AlNbO_4$. Sensitivity is greatly dependent on the amount of chemisorbed oxygen. When the concentration of ethanol gas in air was the same, the maximum sensitivity was obtained at 250 °C. This may be attributed to the availability of sufficient adsorbed ionic species of oxygen on the sensor surface which react most effectively with ethanol molecules at this particular temperature. Selectivity is an important parameter of gas sensors and it is the ability of a sensor to respond to a certain gas in presence of other gases. Theoretically, the sensors should have high response to some gases and little or no response to other gases in the same surroundings. At the given experimental conditions, the response of the sensor to ethanol is high, indicating that the $AlNbO_4$ based sensor has a good selectivity to ethanol among the examined gases. The overall reactions of ethanol vapour, LPG and $NH_3$ and chemisorbed oxygen species are follows [20];

$$C_2H_5OH + O_2 \rightarrow CH_3CHO + H_2O$$

$$CH_3CHO + 5O^-_{(ads)} \rightarrow 2CO_2 + 2H_2O + 5e^-$$

$$2C_nH_{2n+2} + 2O_2{}^- \rightarrow 2C_nH_{2n}O + 2H_2O + 2e^-$$

$$2NH_3 + 3O^-_{(ads)} \rightarrow N_2 + 3H_2O + 3e^-$$

From the above typical reactive formulas, it can be found that, to the same concentration of target gases, ethanol released more electrons than other gases. This may be the reason but not the only reason why $AlNbO_4$ based sensor has good ethanol sensing property. Also further research is needed to explain the good selectivity of the sensor to ethanol among the examined gases.

### 4.3. Sensor response with gas concentrations

Fig. 11 shows the relationship between sensor response and gas concentrations for a sensor operated at 250 °C. The $AlNbO_4$ based sensor element exhibited significant increase in sensitivity even at lower concentrations of ethanol. The sensitivity increased linearly with increase in gas concentration up to 600 ppm. It was observed that the gas had a tendency to get saturation at gas concentrations above 600 ppm. The response of a sensor depends on removal of adsorbed oxygen molecules by reaction with the target gas and generation of electrons. For a small concentration of gas exposed on a fixed surface area of the sample, there was a lower coverage of gas molecules on the surface and hence lower surface reaction occurred. An increase in gas concentration, increased the surface

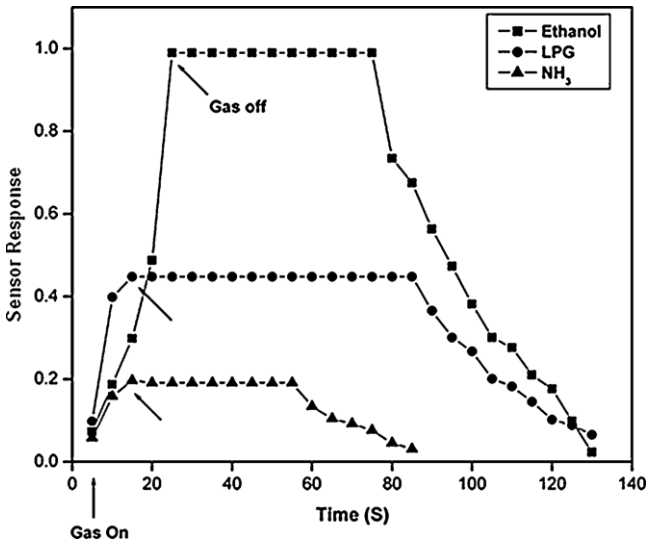


**Fig. 12.** Response of $AlNbO_4$ sensor as a function of time at their optimum operating temperatures for $C_2H_5OH$, LPG and $NH_3$ gases.

reaction due to larger surface coverage. On further increases in concentration of test gas, the surface reaction got saturation due to complete coverage of the gas molecules. The response to 600 ppm of $C_2H_5OH$ was higher than that to 600 ppm of LPG and $NH_3$ suggesting that $AlNbO_4$ based sensor had good sensitivity to $C_2H_5OH$.

### 4.4. Sensor with time

The response time is defined as the time taken to reach the maximum change in sensor-resistance, when the requisite amount of test gas is introduced into the test chamber. The recovery time is defined as the time taken to return to the base resistance when the gas is turned off at the optimum operations temperature. Fig. 12 gives the response and recovery time of $AlNbO_4$ at an operating temperature 250 °C, when exposed to reducing gas. When ethanol gas was introduced, the response of the sensor increased, and the response time to reach the maximum response was less than 24 s. After the ethanol gas was removed, the response gradually decreased, and the recovery time to restore original value from the maximum response was less than 100 s. The response and recovery time for $NH_3$ and LPG about 15, 15 s and 109, 64 s, respectively.

## 5. Conclusions

$AlNbO_4$ nanopowder could be synthesized by the niobium–citrate process. The XRD pattern of $AlNbO_4$ confirmed orthorhombic structure. SEM and TEM analyses showed the porous nature of the nanopowder and the average size of the rectangle shaped $AlNbO_4$ nanopowder was 30 nm in width and 60 nm in length, respectively. EDX result had good agreement with the nominal composition. The temperature dependence of conductance followed Arrhenius relation. Diffuse reflectance spectra revealed that the optical band gap of $AlNbO_4$ was 3.63 eV. The gas-sensing behaviour of $AlNbO_4$ based sensor was examined at the temperatures between 50 and 350 °C. $AlNbO_4$ nanopowder had n-type behaviour and good sensitivity towards ethanol compared to the other two reducing gases (LPG and $NH_3$) at an operating temperature of 250 °C. This sensor is very promising for ethanol detection in the low ppm range, with a response time in second range.

## Acknowledgements

The authors thank The Head, Department of Metallurgical and Materials Science, Indian Institute of Technology (I.I.T) Madras for providing the TEM facility.

## References

[1] S.H. Mujawar, A.I. Inamdar, C.A. Betty, V. Ganesan, P.S. Patil, Electrochim. Acta 52 (2007) 4899.
[2] R. Romero, J.R. Ramos-Barrado, F. Martin, D. Leinen, Surf. Interface Anal. 36 (2004) 888.
[3] T. Weber, R. Andrade, E. Rheite, E. Longo, Sens. Actuators B Chem. 72 (2001) 180.
[4] A. Kohli, C.C. Wang, S.A. Akbar, Sens. Actuators B Chem. 56 (1999) 121.
[5] X. Chen, T. Yu, X. Fan, H. Zhang, Z. Li, J. Ye, Z. Zou, 253, Appl. Surf. Sci. (2007) 8500.
[6] R. Theissmann, H. Ehrenberg, H. Weitzel, H. Fuess, Solid State Sci. 7 (2005) 791.
[7] J.C.P. Flores, F. Garcia-Alvarado, Solid State Sci. 11 (2009) 207.
[8] S. Wongsaenmai, R. Yimnirun, S. Ananta, J. Mater. Sci. 42 (2007) 3754.
[9] F. Vullum, T. Grande, Solid State Ionics 179 (2008) 1061.
[10] J.R. Tolchard, H. Lea Lein, T. Grande, J. Eur. Ceram. Soc. 29 (2009) 2823.
[11] K. Bhattacharyya, A.K. Tyagi, J. Alloys Compd. 470 (2009) 580.
[12] S.V. Jagtap, A.V. Kadu, V.S. Sangawar, S.V. Manorama, G.N. Chaudhari, Sens. Actuators B Chem. 131 (2008) 290.
[13] PCPDFWIN Version 2.4, JCPDS-ICDD, 2003.
[14] S. Esther Dali, M.J. Chocklingam, Mater. Chem. Phys. 70 (2001) 73.
[15] K.M. Abraham, Z. Jiang, B. Carroll, Chem. Mater. 9 (1997) 1978.
[16] M. Watanabe, K. Sanui, N. Ogata, T. Kobayashi, Z.O. Htaki, J. Appl. Phys. 57 (1985) 123.
[17] V.V. Atuchin, I.E. Kalabin, V.G. Kesler, N.V. Pervukhina, J. Elect. Spect. Rel. Phenom. 142 (2005) 129.
[18] M.S. Wagh, G.H. Jain, D.R. Patil, L.A. Patil, Sens. Actuators B Chem. 122 (2007) 357.
[19] J. Cerda Belmonte, J. Manzano, J. Arbiol, A. Cirera, J. Puigcorbe, A. Vila, N. Sabate, I. Gracia, C. Cane, J.R. Morante, Sens. Actuators B Chem. 144 (2006) 881.
[20] P.P. Sahay, R.K. Nath, Sens. Actuators B Chem. 133 (2008) 222.